

# Minimization of Tool Tracking Error using Fulcrum Correction in Minimally Invasive Interventions: Application to Prostate Biopsy Procedure

Derek Cool<sup>a,b</sup>, Shi Sherebrin<sup>a</sup>, Jonathan Izawa<sup>c</sup>, Terrence Peters<sup>a,b</sup> and Aaron Fenster<sup>a,b</sup>

<sup>a</sup>Robarts Research Institute, 100 Perth Dr., London, ON, Canada;

<sup>b</sup>Department of Medical Biophysics, University of Western Ontario, London, ON, Canada;

<sup>c</sup>Department of Surgery and Oncology, Division of Urology, UWO, London Health Sciences Centre, London, ON, Canada

## ABSTRACT

Real-time 3D optical tracking of free-hand imaging devices or surgical tools has been studied and employed for object localization in many minimally invasive interventions. However, the surgical workspace for many interventional procedures is often sub-dermal with tool access through ports from surgical incisions or anatomical orifices. To maintain the optical line-of-sight criterion, external extensions of inserted imaging devices and rigid surgical tools must be tracked to localize the internal tool tips. Unfortunately, tracking by this form of correspondence is very susceptible to noise as orientation errors on the external tracked end compound into both rotational and translational errors on the internal, workspace position. These translational errors are proportional to the length of the probe and the sine of the angulation error, so small angulation errors can quickly compromise the accuracy of the tool tip localization.

We propose a real-time tracking correction technique that uses the rotational fulcrum created by the device entry port to minimize the effect of translational and rotational noise errors for tool tip localization. Our technique could apply to many types of interventions, but we focus on the application to the prostate biopsy procedure for tracking a transrectal ultrasound (TRUS) probe commonly used for prostate biopsies. In vitro studies were performed using the Claron Technology MicronTracker 2 to track a TRUS probe in a fixed rotational device. Our experimental results showed an order of magnitude improvement in RMS localization of the internal TRUS probe tip using fulcrum correction over the raw tracking information.

**Keywords:** Image-guided surgery, tracking, optical tracking, fulcrum, rotational point, prostate biopsy

## 1. INTRODUCTION

3D free-hand tracking of imaging devices and surgical tools has been used during minimally-invasive, image-guided surgeries and therapies (IGST) to provide real-time feedback on the locations and orientations of medical instruments intra-procedure.<sup>1-6</sup> Accurate tool tracking is difficult for many of these procedures, because the clinical work space is often located beneath the skin and is not visible by a clear line of sight. Micro-magnetic trackers can be used to provide tool tip information within the body; however, attaching the markers to a probe that permits full movement and prevents the probe & tracking marker from separating is not always trivial. Also, ferromagnetic objects and external magnetic fields have been shown to distort the tracker workspace and limit the accuracy of magnetic trackers.<sup>7-9</sup>

While optical tracking is not affected by problems related to magnetic fields, it introduces a line-of-sight criterion between the camera and tracking marker. As a result, tools must use correspondence tracking, by attaching tracking markers to the external portion of the probe and inferring the tool-tip location based on a predetermined calibration transform that maps points from the tracking marker to the tool tip. As illustrated in Figure 1, this technique has its own limitations, since errors in evaluating the marker position and orientation

---

Further author information: (Send correspondence to D.Cool)

D.Cool.: E-mail: dcool@imaging.robarts.ca, Telephone: 1 519 663 5777 x34278

A.Fenster.: E-mail: afenster@imaging.robarts.ca

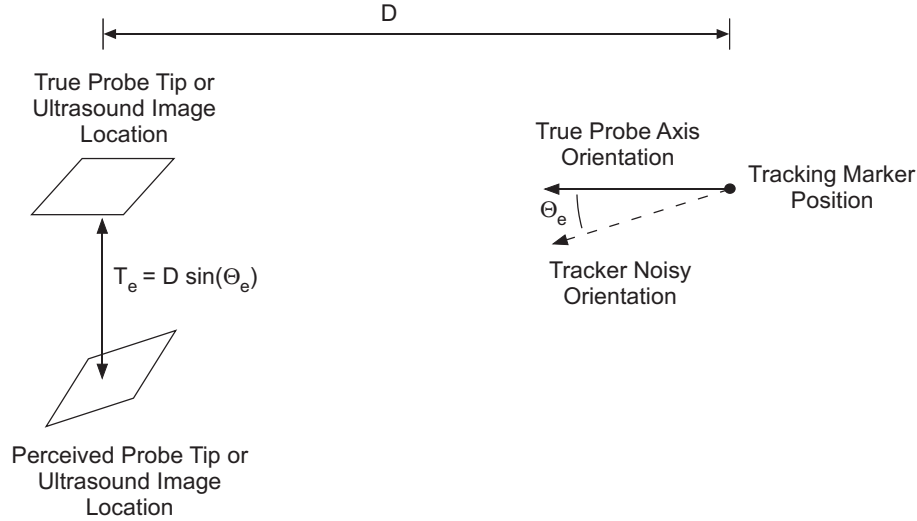


**Figure 1.** Illustration of the compounding error of resulting from tracking noise in the marker orientation when using correspondence tracking.

compound into both orientation and translational errors at the probe effector end. This translational error,  $T_e$ , is roughly proportional to the probe length,  $D$ , and the sine of the angle of error,  $\theta_e$ ;  $T_e \cong D \sin(\theta_e)$ . Therefore, a  $1^\circ$  error at the marker can translate into a 5 mm error at the end of a 30 cm probe.

Almost all IGST procedures gain access to the internal clinical target through either surgical or natural entry ports into the body. A number of these procedures (thoracic & abdominal surgeries, prostate biopsies, etc.) use the entry port as a rotational fulcrum for the imaging probes or surgical tools. Since the main axis of the probe must always be directed through this fulcrum, knowledge of the fulcrum position and probe axis could be used to correct the position and orientation of the tracked marker during free-hand movement. “Constraining” the marker based on a known fulcrum location could decrease the compounding effect of rotational errors and actually lead to a decrease in the overall error at the target end of the probe.

In this paper, we propose an fulcrum-based tracking correction algorithm that has application to IGST procedures involving a rotational entry port. Our algorithm is ideal for free-hand tool movement as it is invariant to marker orientation and insertion depth. The algorithm was tested using the MicronTracker 2 (Claron Technology, Toronto, Canada) with markers attached to a transrectal ultrasound (TRUS) probe commonly used in the prostate biopsy procedure.

## 2. METHODS

### 2.1. Fulcrum Position and Probe Axis Calculation

Prior to probe tracking, the fulcrum correction algorithm requires that the fulcrum position,  $X_F$ , be known in the 3D world space, and that the main axis of the probe be known in marker space coordinates (see Fig. 2). Since the primary probe axis vector is contained within the probe/marker space, its calibration is only required when the marker’s position or orientation is moved relative to the probe and therefore, not be calibrated prior to each procedure. The fulcrum position, however, must be recalculated whenever its position moves relative to the tracking camera (which would likely be for each procedure).

The fulcrum position can be determined in one of at least two ways. The first is achieved by attaching a tracking marker to the rotational fulcrum itself. This would allow movement of the fulcrum without compromising the integrity of the correction algorithm. For the second option, and that used in this experiment, the fulcrum position is determined during the procedure, by rotating a tracked tool at a constant insertion depth and solving for the least-squares intersection point of the collected transforms, as is commonly used for stylus probe

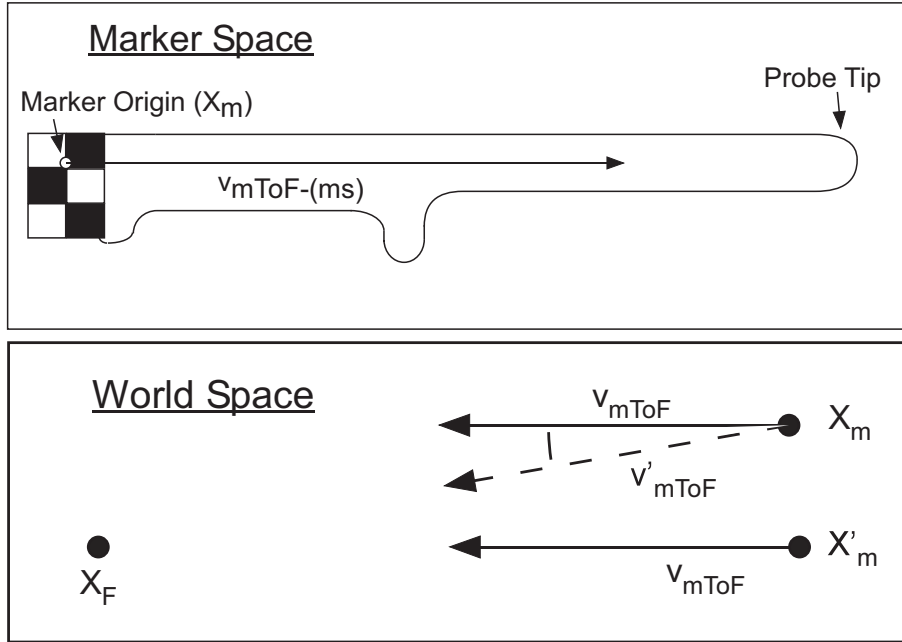


**Figure 2.** Illustration of the vectors and positions associated with the fulcrum correction algorithm in marker space (top) and world space (bottom). From top,  $v_{mToF-(ms)}$  represents the marker origin-to-fulcrum vector relative to the probe or marker space geometry. In the bottom diagram,  $X_F$  represents the fulcrum position in world space,  $X_m$  and  $v_{mToF}$  respectively represent the marker origin and marker-to-fulcrum vector inputted from the tracking device, and  $X'_m$  &  $v'_{mToF}$  represent the expected marker origin and marker-to-fulcrum vector, respectively, given the  $X_F, X_m$ , &  $v_{mToF}$ .

calibrations. Using this technique, it is assumed that the fulcrum position remains constant throughout the remainder of the procedure; otherwise, the fulcrum calibration must be repeated.

The probe axis can also be easily determined by simply calculating the fulcrum rotation point in marker space for two insertion depths for the probe. This should provide at least 2 points (along the probe axis) within the marker space, which define the vector of the probe axis. For this experiment, since we were using an “end-firing” TRUS biopsy probe, the axis of the probe is assumed to be parallel to the y-axis of the TRUS image. Calibration of the tracking marker with the TRUS image was performed using Gobbi’s “Z-bar” calibration phantom.<sup>10</sup>

## 2.2. Fulcrum Correction Algorithm

During real-time tool tracking, the fulcrum position,  $X_F$ , is assumed to be fixed or is independently tracked so that its 3D location in world space is known at all times. This is important as the world space must be transformed so that it is always centered around the fulcrum. Also, it is assumed that the marker origin,  $X_m$ , has been calibrated so that it is located along the axis of the probe. This requirement is necessary to ensure that the algorithm is invariant to insertion depth of the probe.

The tracked marker location matrix,  $M$ , provides a snapshot of the marker position and orientation at a specific moment in time. The matrix can be decomposed into:

$$M = \begin{bmatrix} R & X_m \\ 0 & 0 & 0 & 1 \end{bmatrix}; \text{ where } R \in \mathbb{R}^{3 \times 3}, X_m \in \mathbb{R}^3$$

where  $R$  represents the rotation matrix for orientation of the marker space; and  $X_m$  represents the marker position in world space (see Fig. 2). Through matrix multiplication of the orientation transform,  $R$ , with the probe axis vector in marker space,  $v_{mToF-(ms)}$ , the probe axis is defined in world space coordinates,  $v_{mToF}$ :

$$v_{mToF} = R v_{mToF-(ms)} \quad (1)$$

Based on the tracked marker location,  $X_m$ , and the calculated fulcrum position,  $X_F$ , the expected probe axis vector,  $v'_{mToF}$ , and the distance from the marker to the fulcrum,  $d'_{mToF}$ , is calculated by:

$$v'_{mToF} = \frac{X_F - X_m}{|X_F - X_m|} \quad (2)$$

$$d'_{mToF} = |X_F - X_m| \quad (3)$$

$v'_{mToF}$  provides the expected direction of the probe axis vector given the tracked marker position and the known fulcrum location (see Fig. 2).  $d'_{mToF}$  estimates how far the probe has been inserted so that this value can be maintained throughout the correction.

In addition to the expected probe axis vector, an expected marker location,  $X'_m$ , is determined based on the position of the fulcrum (assumed previously to be the origin), the world space probe axis vector,  $v_{mToF}$ , and the probe insertion distance,  $d'_{mToF}$ :

$$X'_m = X_F + d'_{mToF}(-v_{mToF}) \quad (4)$$

$X'_m$  and  $R$  are combined to form a new matrix,  $M'$ :

$$M' = \begin{bmatrix} R & X'_m \\ 0 & 1 \end{bmatrix}; \text{ where } X'_m \in R^3$$

A rotation is then applied to  $M'$  to produce the final corrected matrix  $M''$ :

$$M'' = R(w)M'; \text{ where } R(w) \in R^{3 \times 3}, \quad (5)$$

where  $R(w)$  is the rotation matrix formed by rotating  $\theta(w)$  degrees about the vector formed by  $v_{mToF} \times v'_{mToF}$ .  $\theta(w) = w\theta$  where  $w$  represents a user-defined ‘‘correction parameter’’,  $0 \leq w \leq 1$ , that modulates the degree of rotation, such that as  $w \rightarrow 0$ ,  $M'' \rightarrow M'$  and as  $w \rightarrow 1$ , the transform is rotated to the original inputted marker position  $X_m$  with the orientation rotated so that the probe axis =  $v'_{mToF}$  and is directed toward the fulcrum point,  $X_F$ .

### 2.3. Experimental Design

Motion tracking tests were performed using the MicronTracker 2 (Claron Technology, Toronto, Canada) to monitor a marker attached to the handle of an ‘‘end-firing’’ TRUS biopsy probe and the probe was mounted in a rotational device. The rotational fulcrum was positioned 23 cm from the tracking markers on the probe, at a point corresponding approximately to the insertion depth for prostate biopsies. The distance from the marker to the ultrasound transducer was approximately 30 cm.

The world-space fulcrum position was calculated by rotating the probe about two orthogonal axes, around  $\pm 20^\circ$  at a fixed distance and computing the intersection point of all the collected transforms using least-squares estimation. The probe was then fixed in a stationary, vertical position and 100 transforms of the probe marker location were captured. Both the fulcrum position and the uncorrected (or ‘‘raw’’) transforms were stored and off-line evaluation was performed to compute the root-mean-square (RMS) error of both raw and corrected transforms. The mean of the original, uncorrected transforms was used as the ‘‘true’’ transform value for the tracking marker position and orientation. Fulcrum corrections were performed for each transform, using correction parameters  $w = [0, 0.1, 0.2, \dots, 1.0]$ .

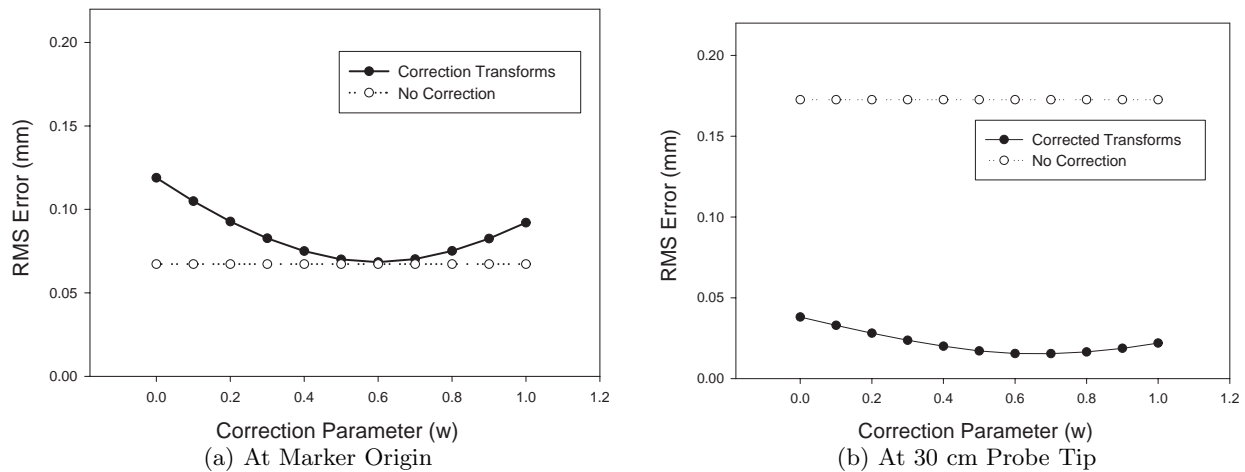


**Figure 3.** Plot of the RMS Error at (a) the tracking marker, (b) 30 cm length of the probe.

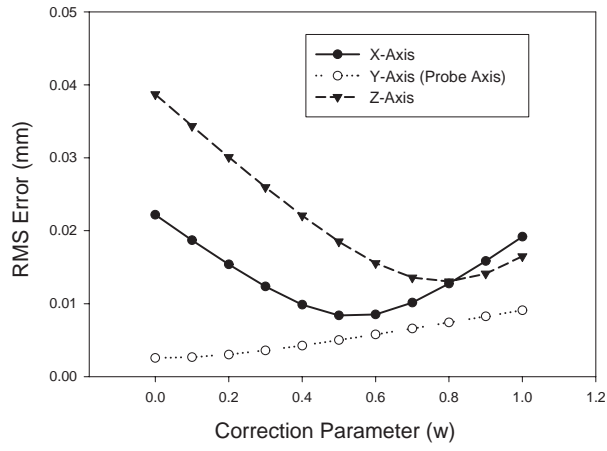
### 3. RESULTS

At the marker origin,  $X_m$ , the overall RMS error of the raw, uncorrected transforms was  $0.067\text{ mm}$ . Correcting the transforms using the fulcrum correction algorithm did not decrease the RMS error for any of the input correction parameters, and the lowest error was seen for  $w = 0.6$  with an RMS error of  $0.068\text{ mm}$  (see Fig. 3(a)). When the RMS error was calculated at probe tip point of 30 cm from the marker origin, which approximately corresponds to the base of the TRUS biopsy image, all fulcrum parameter values showed a decrease in the RMS error (see Fig. 3(b)). Fulcrum correction with  $w = 0.7$  showed an order of magnitude improvement in RMS over the uncorrected results at 30 cm, with values of  $0.015\text{ mm}$  &  $0.17\text{ mm}$  respectively for the corrected and uncorrected transforms.

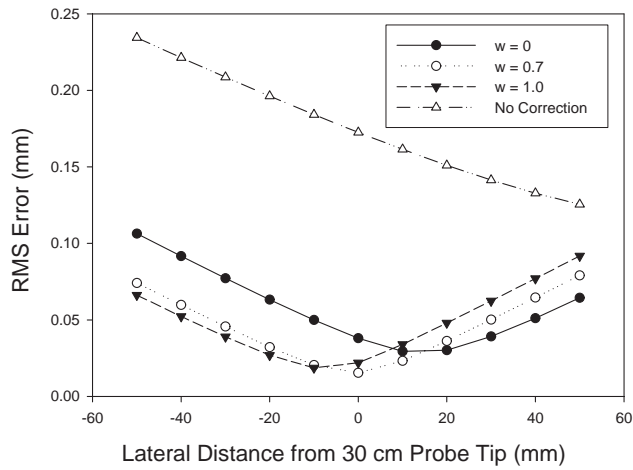
When the RMS error at the 30 cm probe tip position was decomposed into the primary world space axes, different results were found for each of the x, y, & z axes (See Fig. 4). Also, the fulcrum correction parameter,  $w$ , affected each axes differently as the slope of the curves and the range of RMS values varied between the axes. In the y-axis direction, which is approximately parallel to the probe axis, the RMS curve was nearly linear and had the smallest range of RMS values, going from the minimum of  $0.0026\text{ mm}$  for  $w = 0.0$  to the maximum of  $0.0091\text{ mm}$  for  $w = 1.0$ . The x-axis showed more of a parabolic curve with a minimum of  $0.0084\text{ mm}$  at  $w = 0.5$  and a maximum of  $0.022\text{ mm}$  at  $w = 0.0$ . Finally, the z-axis direction had the largest range of RMS values, going from  $0.013\text{ mm}$  for  $w = 0.8$  to  $0.039\text{ mm}$  for  $w = 0.0$ .

Figure 5 plots the RMS error at different points perpendicular to the probe long axis at a probe distance of 30 cm. These points correspond to points along the x-axis of the TRUS image. Through the entire extent of the TRUS image width (approximately 10 cm), the RMS error for the transforms corrected using the fulcrum correction algorithm was lower than those uncorrected. Each of the fulcrum correction parameters,  $w$ , had a hyperbolic curve, with a minimum located within  $\pm 1\text{ cm}$  of the probe tip. The RMS error curve minima started at 1 cm from the probe tip for  $w = 0.0$ , with an RMS error of  $0.029\text{ mm}$ . As the fulcrum parameter was increased, the minima values moved toward and through the probe tip, finishing at -1 cm for  $w = 1.0$ , with a RMS error of  $0.019\text{ mm}$ . For all parameter values for the fulcrum correction and across all the TRUS distances, the minimum RMS value was  $0.015\text{ mm}$  found at the probe tip for  $w = 0.7$ .

Finally, the effect of an error in the fulcrum position was calculated by adding a translational error to the calculated fulcrum position prior to running the fulcrum correction with  $w = 0.7$ . As seen in Figure 6, errors in fulcrum localization, in directions perpendicular to the probe axis, increase the overall RMS error at the probe tip.



**Figure 4.** Plot of the RMS error associate with each world space axis. The RMS calculations were done at a probe tip distance of 30 cm from the tracking marker origin. Note: The y-axis roughly corresponds to the long axis of the probe.



**Figure 5.** Plot of the RMS Error at lateral positions off of the probe tip at 30 cm.

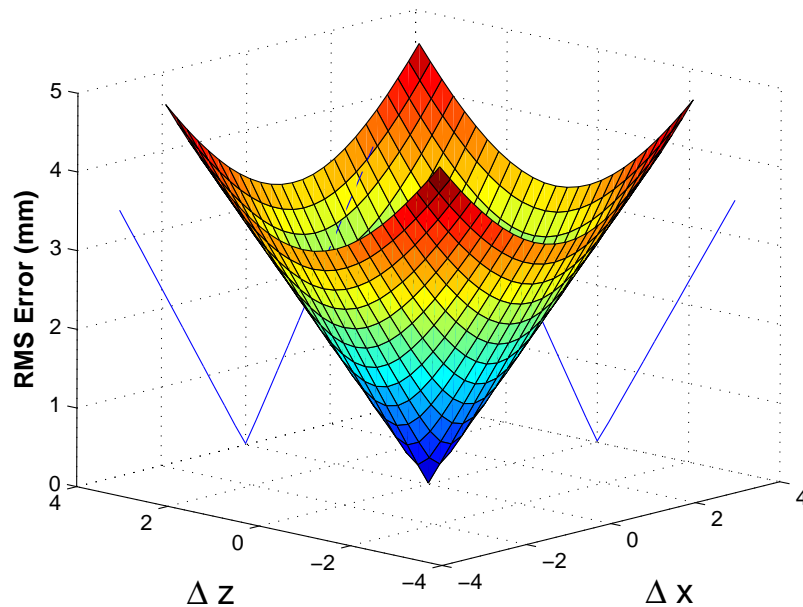


**Figure 6.** 3D Plot of how the RMS error changes as an error is added to the the fulcrum position. The 2D projection of the RMS error curve has been drawn onto both the xz and yz graphing planes.

#### 4. DISCUSSION

The results from this work suggest that using a fulcrum as an added constraint or correction tool can greatly decrease the RMS error of the probe tip location. In the case of the TRUS probe, an order of magnitude improvement in the RMS error was achieved using the fulcrum correction parameter of  $w = 0.7$ , which proved to be the optimal parameter from our results; however the fulcrum parameter values affect each major axis differently, suggesting that modifying the algorithm to provide axis-specific correction parameters might allow further optimization and reduction of RMS error. Finally, the application of fulcrum correction is in question as the procedure is done without sedation of the patient and simulated tests have shown that movement or errors in knowledge of the fulcrum position quickly eliminate the gains obtained from using the fulcrum correction technique. In spite of this, our results show the potential of this technique to minimize probe tip localization errors for many forms of minimally-invasive, image-guided surgeries and therapies.

#### ACKNOWLEDGMENTS

The authors would like to thank Anis Ahmad for his help in reviewing the conceptual aspects of this work and Greg Mills for his help in the design and construction of the rotational device. This research work has supported by funding from the Canadian Institute of Health Research (CIHR) and the Prostate Cancer Foundation.

#### REFERENCES

1. F. Banovac, J. Tang, S. Xu, D. Lindisch, H. Y. Chung, E. B. Levy, T. Chang, M. F. McCullough, Z. Yaniv, B. J. Wood, and K. Cleary, "Precision targeting of liver lesions using a novel electromagnetic navigation device in physiologic phantom and swine," *Med Phys* **32**(8), pp. 2698–705, 2005.
2. P. Bao, J. Warmath, J. Galloway, R., and A. Herline, "Ultrasound-to-computer-tomography registration for image-guided laparoscopic liver surgery," *Surg Endosc* **19**(3), pp. 424–9, 2005.

3. R. M. Comeau, A. F. Sadikot, A. Fenster, and T. M. Peters, "Intraoperative ultrasound for guidance and tissue shift correction in image-guided neurosurgery," *Med Phys* **27**(4), pp. 787–800, 2000. 0094-2405 (Print) Case Reports Journal Article.
4. R. Ewers, K. Schicho, G. Undt, F. Wanschitz, M. Truppe, R. Seemann, and A. Wagner, "Basic research and 12 years of clinical experience in computer-assisted navigation technology: a review," *Int J Oral Maxillofac Surg* **34**(1), pp. 1–8, 2005.
5. S. C. Gebhart, E. D. Jansen, and R. L. Galloway, "Dynamic, three-dimensional optical tracking of an ablative laser beam," *Med Phys* **32**(1), pp. 209–20, 2005.
6. G. M. Guiraudon, D. L. Jones, A. C. Skanes, D. Bainbridge, C. M. Guiraudon, S. M. Jensen, X. Yuan, M. Drangova, and T. M. Peters, "En bloc exclusion of the pulmonary vein region in the pig using off pump, beating, intra-cardiac surgery: a pilot study of minimally invasive surgery for atrial fibrillation," *Ann Thorac Surg* **80**(4), pp. 1417–23, 2005.
7. W. Birkfellner, F. Watzinger, F. Wanschitz, G. Enislidis, C. Kollmann, D. Rafolt, R. Nowotny, R. Ewers, and H. Bergmann, "Systematic distortions in magnetic position digitizers," *Med Phys* **25**(11), pp. 2242–8, 1998.
8. J. S. Day, D. J. Murdoch, and G. A. Dumas, "Calibration of position and angular data from a magnetic tracking device," *J Biomech* **33**(8), pp. 1039–45, 2000.
9. J. Hummel, M. Figl, C. Kollmann, H. Bergmann, and W. Birkfellner, "Evaluation of a miniature electromagnetic position tracker," *Med Phys* **29**(10), pp. 2205–12, 2002.
10. D. Gobbi, R. Comeau, and T. Peters, "Ultrasound probe tracking for real-time ultrasound/mri overlay and visualization of brain shift," in *Medical Image Computing and Computer-Assisted Intervention - MICCAI'99*, C. Taylor and A. Cholchester, eds., *Lecture Notes in Computer Science* **1679**, pp. 920–927, Springer, (Cambridge, UK), 1999.